Hydrokinetic turbines in yawed conditions: towards synergistic fluvial installations

Mirko Musa [1] Giulia Ravanelli [2] Walter Bertoldi [3] Michele Guala [4]

ABSTRACT

Laboratory experiments were performed in critical mobility conditions to study the effects of an in-stream horizontal axis turbine in yawed conditions. The misalignment between the rotor axis and the incoming flow velocity is observed to alter the near and far wake of the turbine, as well as the scour and deposition patterns in the proximity of the monopile support tower. Various hydraulic conditions may lead to such misalignment: as a result of complex fluvial bathymetries distorting the flow, or as a strategy to steer the wake away from downstream units and maximize energy production in a turbine array. The research first investigates the simplest case, with a single turbine deployed along the channel centerline and oriented at different yaw angles, to study the wake deflection and the turbine performance. A second set of experiments is performed moving the turbine relatively close to a non-erodible lateral wall to explore a potential passive yaw control strategy devoted to protect the banks from erosion by steering the

[1]St. Anthony Falls Laboratory, Department of Civil, Environmental, and Geo- Engineering, University of Minnesota, 2 SE 3rd Ave, Minneapolis, MN 55414. E-mail: mmusa@umn.edu

[2]Department of Civil, Environmental, and e Mechanical Engineering, University of Trento, Via Mesiano, 77, 38123, Trento, Italy; and St. Anthony Falls Laboratory, Department of Civil, Environmental, and Geo- Engineering, University of Minnesota, 2 SE 3rd Ave, Minneapolis, MN 55414. E-mail: giulia.ravanelli@alumni.unitn.it

[3]Department of Civil, Environmental, and e Mechanical Engineering, University of Trento, Via Mesiano, 77, 38123, Trento, Italy. E-mail: walter.bertoldi@unitn.it

[4]St. Anthony Falls Laboratory, Department of Civil, Environmental, and Geo- Engineering, University of Minnesota, 2 SE 3rd Ave, Minneapolis, MN 55414. E-mail: mguala@umn.edu

wake towards the channel center and favor deposition along the bank.

Keywords: In-stream Turbines, Yaw, Renewable energy, Streambank protection, River, Erosion, Sediment

INTRODUCTION

In the last decade feasibility studies and resource assessments for the deployment of Marine and Hydrokinetic (MHK) devices in tidal, estuarine, or fluvial environments have increased significantly (Haas et al. 2011; Jacobson et al. 2011; Baldwin et al. 2015; Muljadi and Yu 2015; Bane et al. 2017; National Renewable Energy Laboratory (NREL)). It is therefore very important to understand the long term effects that these devices may have on the ecological and morphodynamic equilibrium of the river, as well as the more immediate effects that changes in fluvial bathymetry may have on the safety and performance of the device (Neill et al. 2009; Yang and Copping 2017; Fraser et al. 2017; Nash and Phoenix 2017; Ramírez-Mendoza et al. 2018). Most of the experiments and numerical studies, so far, have focused mainly on characterizing the turbulence and the wake structure (Myers and Bahaj 2007; Maganga et al. 2010; Kang et al. 2012; Churchfield et al. 2013; Lam et al. 2015; Bachant and Wosnik 2015a; Morandi et al. 2016; Lust et al. 2018), the turbine response to turbulent flow conditions (Neary et al. 2013; Chamorro et al. 2013; Stallard et al. 2013; Ahmadi 2019), and the power production capabilities of these devices (Myers and Bahaj 2006; Bahaj et al. 2007; Bachant and Wosnik 2015b; Strom et al. 2017). More recently, the geomorphic effects of the turbine on the erodible riverbeds have been investigated, characterizing the scour and deposits forming downstream of the turbine. Hill et al. (2014) quantified experimentally (later on simulated numerically by Yang et al. (2017)) the interactions between hydrokinetic turbines and the erodible sediment layer in an open channel flow, estimating the scour augmentation due to the spinning turbine rotor as opposed to the typical bridge pier scour occurring at the base of the monopile foundation tower (see

also Chen et al. (2017)). Later, the mutual interaction between the turbines and migrating dunes was identified in a straight channel flow (Hill et al. 2016b) and in a meandering stream (Hill et al. 2016a). The major outcomes are a weak performance modulation due to the shear layers developing over the dunes and impinging the rotor (Hill et al. 2016b), and a slight wake distortion affecting the secondary flow in the meandering channel and altering the transverse slope (Hill et al. 2016a). The latter work provided the inspiration to investigate how MHK rotor misalignment with respect to the incoming flow can be used to steer the wake at minimal performance cost. The potential goals are very interesting from a streambank erosion protection perspective: the near wake is delimited by the tip vortex structure and the corresponding annular shear layer, which represents a highly turbulent and coherent region extending up to three-five diameters downstream of the rotor (3-5 d_T), see for example Kang et al. (2014). As the wake expands and this flow region interacts with the erodible riverbed directly, by impinging tip vortices, or indirectly, by accelerating the flow underneath, augmented localized erosion occurs near the tower foundation (Musa et al. 2018a). The same erosive mechanism may occur at the stream banks, in case MHK turbines are deployed along the outer meanders thalweg to harvest more kinetic energy (Hill et al. 2016a). An opportunity to mitigate streambank erosion is to employ a yawed rotor configuration, potentially steering the flow towards the center of the channel (similarly to other traditional protection strategies (Odgaard and Mosconi 1987; Odgaard and Wang 1991a; Shields Jr et al. 2003; Abad et al. 2008; Khosronejad et al. 2013, among others)). Controlling the wake of axial flow turbines is a well known strategy to maximize wind power performance at the wind farm scale by enhancing mixing and high momentum fluid entertainment in the wakes (Gebraad et al. 2017; Boersma et al. 2017). More specifically, a minimal yaw angle misalignment allows steering the upwind turbine wake away from the downwind rotors, providing the incoming flow direction is steady. For wind energy in the atmospheric surface layer this is a

challenging practice, requiring real-time control (Boersma et al. 2017); however in fluvial environments, the stream direction is fairly invariant, implying that small angles can be accurately imposed without continuous yaw adjustments. Several studies have been focused on the performance of yawed wind turbine and their wake characteristics with particular emphasis on the streamwise location of the velocity minima (Grant et al. 1997; Medici and Alfredsson 2006; Bastankhah and Porté-Agel 2016; Dou et al. 2019a, among other). Recently, this investigation was extended to hydrokinetic turbines (Galloway et al. 2014; Frost et al. 2015; Piano et al. 2017; Modali et al. 2018), without however taking into account the erodible riverbed. In an effort to promote the integration of this technology to fluvial environments, this study explores how the yaw angle can steer the wake flow, the scour region and the deposit in the turbine wake. This is investigated experimentally using miniature MHK turbine models deployed both at the center of the channel and near the bank. A potential configuration of interest for the protection of the banks at minimal performance cost is presented and discussed as proof of concept, in broad terms addressing issues of renewable energy production and streambank erosion.

In the next section the reference system and main variables are defined, and the experimental apparatus is described. Thereafter, results are presented from two sets of experiments: i) with the turbine installed in the middle of the channel cross-section at different yaw angles, ii) with the turbine deployed at one rotor diameter from the non erodible side wall. Discussion and conclusions follow.

EXPERIMENTAL APPARATUS AND BASELINE FLOW CONDITIONS

All the experiments were conducted at the St. Anthony Falls Laboratory, University of Minnesota. A 20 m long, 0.9 m wide tilting flume was used, filled with a 0.2 m thick layer of fairly uniform sand of median diameter $d_{50} = 1.13$ mm ($d_{16} = 0.81$ mm, $d_{84} = 1.44$ mm) and geometric standard deviation of $\sigma_g = 1.33$ (estimated using Parker ()

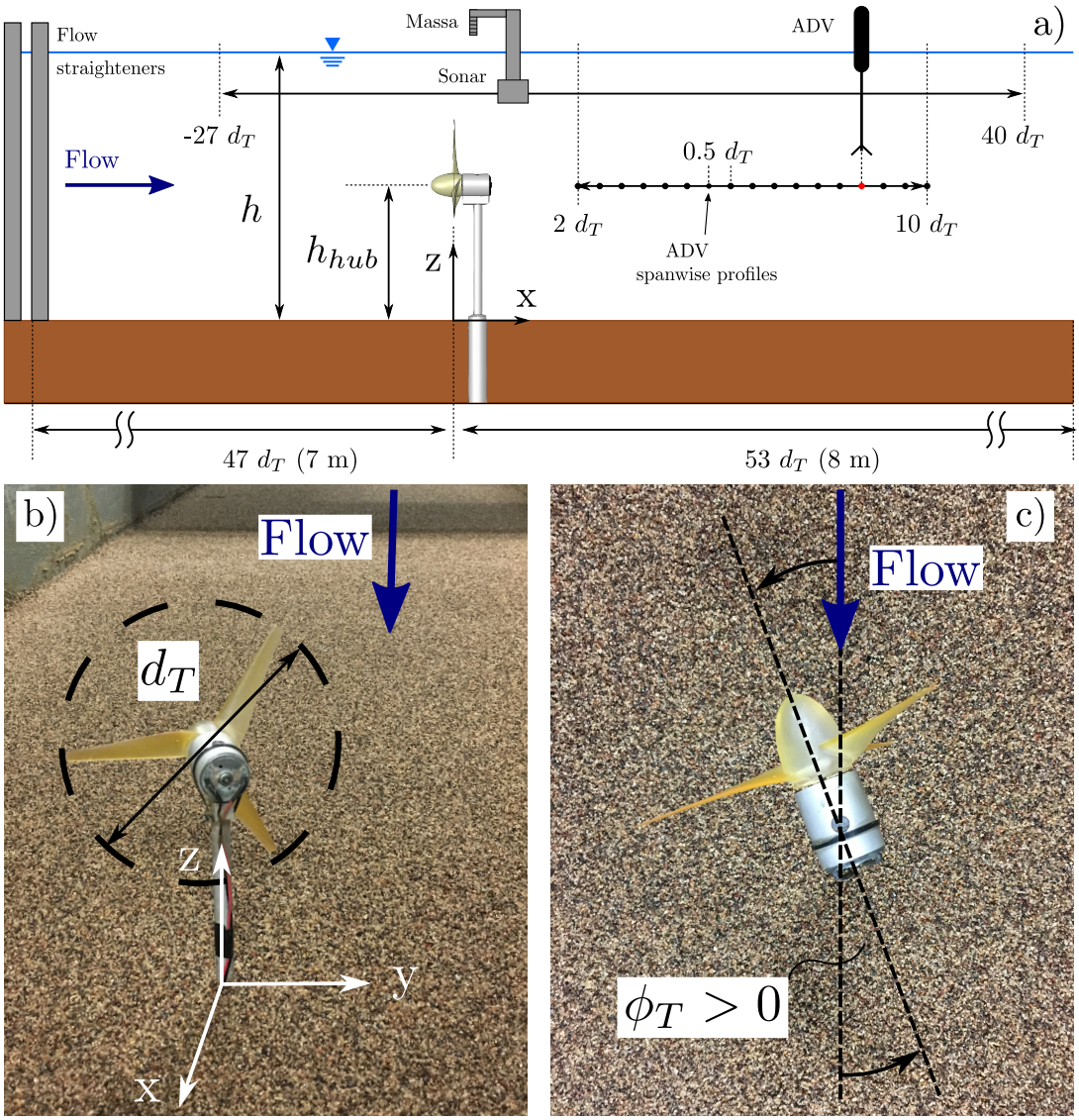

FIG. 1. a) Profile schematic of the experimental set-up, showing inflow boundary conditions, turbine location and part of the measurements range. b) Miniature turbine model (rotor diamter $d_T = 0.15$ m and hub height $h_{hub} = 0.13$ m), and c) turbine orientation reference system.

eBook, Chapter 2).

Flow conditions were defined in order to keep sediments at the threshold of motion,

also defined as critical mobility or clear water, while maintaining the MHK turbine submerged by about half the rotor diameter consistent with Hill et al. (2014). The water discharge was regulated by a calibrated actuating valve, providing continuous supply of water drawn directly from the adjacent Mississippi River. In order to break the large flow structures created by the valve and provide reasonable turbulent intensities at the inlet, the upstream flow is forced through an array of 18 closely spaced vertical cylinders (0.05 m diameter and net spacing), resulting in a fairly spanwise homogeneous flow before entering the test section. Figure 1a shows a schematic view of the experimental setup.

Turbine model

The miniature turbine model used in all experiments is the three blades, axial-flow, MHK model tested by Hill et al. (2014) with rotor diameter $d_T = 0.15$ m, hub height with respect to the undisturbed bed of $h_{hub} = 0.13$ m and 0° pitch angle at the blade tip (see more details in Hill et al. (2014)). The rotor hub and blades were 3D printed and connected through a shaft to a DC motor (model #RK- 370CA-14420), enabling high frequency acquisition of the voltage at 200 Hz (Measurement Computing MiniLAB 1008 USB data acquisition board) as a measure of the turbine instantaneous angular velocity under frictional torque (Howard et al. 2015; Hill et al. 2016b). As demonstrated in Musa et al. (2018b), the voltage signal produced by the three internal rotating copper coils of the DC motor (used here in reverse), is linearly proportional to the rotor angular velocity. The miniature turbine employed here is designed to provide a geometrically scaled representation of a high performance, 0.5 m diameter, turbine (Chamorro et al. 2013) and a reliable streamwise evolution of the scaled wake velocity deficit (Musa et al. 2018b). For the first set of experiments, the turbine model was positioned 7 m downstream of the channel inlet ($x = 0$ coordinate, x being the streamwise direction) in order to have the test section area sufficiently far from the boundary

conditions and thus characterized by an incoming uniform flow, and centered in the channel cross-section ($y = 0$ coordinate, y being the spanwise direction), as shown in Figure 1. For the second set of experiments, the x position was kept invariant, while the turbine was moved closer to the wall $y = 0.3$ m, thus keeping a minimum distance of 0.5 d_T between the rotor tip and the sidewall. The rotor orientation, identified by the yaw angle ϕ_T was varied from -30° to 30°, every 10° (see Figure 1c for the reference system), and it is indicated hereafter with a white line on the topographic scan plots. In selected cases, the rotor was changed in order to compare the effects of clockwise or counterclockwise blade rotations (from the flow prospective, looking downstream).

Data collection

Flow velocity, turbine generated voltage, bed and water surface elevations were collected in time, during all the performed experiments. All the devices, except for the voltage acquisition, were mounted on a computer-controlled data acquisition cart (DAQ), able to move along the x, y axes of the flume, and monitor the spatial and temporal evolution of the erodible bed and water surface elevations. Longitudinal bed elevation profiles were measured continuously in space and time using an immersible Olympus Panametrics C305-SU sonar transducer. Measurements were acquired along the x-axis ($-27 \leq x/d_T \leq 40$), over the turbine spanwise location, coincident with the channel centerline $y = 0$. Measurements were spaced by $\Delta x = 10$ mm in the stream-wise direction (spatial resolution) and each line repeated every $\Delta t = 46$ s (temporal resolution), for the entire duration of the experiment. The water surface was captured simultaneously by a Massa M5000 ultrasonic range sensor with the same resolution. Experiments were conducted for approximately 4-4.5 hours, which was sufficient for the scour depth and the associated deposit peak to reach the equilibrium. Figure 3b shows the time evolution of the bed elevation at $x/d_T = 0.5$ and $y/d_T = 0$ (the first measurable location by the sonar, moving downstream from the rotor plane), revealing

a plateau after $t \approx 130$ min. At the end of each experiment the channel was carefully drained and a high resolution laser topography scan was performed using state-of-the-art, high-resolution, laser scanning device designed and manufactured at SAFL. The scanning system is composed by a SICK Ranger E50 camera, an OPTO 1W continuous laser and a non-cylindrical uniform line lens. The camera captures the spanwise (y) bed elevation profile illuminated by the 1 mm thick laser. An ad-hoc designed calibration procedure converts the outline pixels into the physical coordinates of bed elevation $z(y)$. The camera captures these profiles at consecutive streamwise locations (x) when triggered by the moving DAQ carriage, at a user-specified Δx, constructing the final bathymetry matrix $z(x, y)$. The laser measuring system has a vertical accuracy of 0.5 mm, while the spatial resolution was imposed to $\Delta x = \Delta y = 2$ mm. Figure 3a shows the final bathymetry for the reference centered case $\phi_T = 0°$.

Instantaneous flow velocities were measured using a 3 components Acoustic Doppler Velocimeter (ADV), downlooking probe, sampled at 200 Hz and positioned by the automated cart system. The velocity profiles were collected i) along the vertical profile z-axis at different locations to contribute defining the shear velocity and the bottom shear stress in the undisturbed baseline conditions, 1 m upstream of the turbine, and ii) along the cross-section coordinate y at hub height $z = z_{hub}$ to monitor the wake expansion, deflection, and the maximum velocity deficit. The wake measurements were collected along 12 spanwise transects, moving the ADV along the y-axis from -0.225 m to 0.225 m, at a velocity of 1 $\mathrm{mm\ s^{-1}}$ (see Hill et al. (2016a) for details). The longitudinal spacing of the streamwise wake profiles was 0.5 d_T in the near wake (from 2 d_T to 4.5 d_T) and 1 d_T in the far wake (from 5 d_T to 10 d_T). An example of wake measurements for the centered turbine with 0° yaw angle are shown in Fig. 3c.

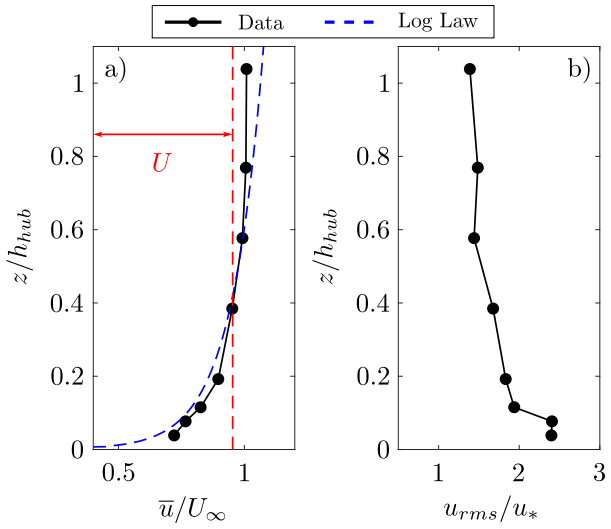

FIG. 2. a) Incoming undisturbed mean velocity profile $\overline{u}(z)$ normalized by the velocity at hub height $U_\infty = 0.42$ ms^{-1}. $U = 0.40$ ms^{-1} represents the depth averaged velocity. b) Streamwise turbulent intensity u_{rms}/u_*, where u_{rms} is the root-mean-square of the streamwise velocity fluctuations and u_* is the shear velocity estimated with the energy method as $u_* = \sqrt{gR_H S_w} = 0.022$ ms^{-1}.

Open channel hydraulic conditions

The flume hydraulic conditions were set to mimic subcritical open channel flows in lowland alluvial systems. The water depth $h = 0.27$ m was controlled by a downstream tail gate; the channel slope and flow discharge were adjusted to provide a streamwise uniform flow, and keep the shear stress at the bed slightly below the critical mobility conditions. Hydraulic parameters and key variables are reported in Table 1.

Preliminary experiments were conducted without the MHK turbine to measure the mean velocity profile and characterize the undisturbed baseline flow. Measurements at 9 points along z, vertical direction, for 5 minutes, sampled at 200 Hz, were collected in the center of the channel, 1 m upstream of the turbine selected location. Figure

2a shows the vertical profile of the mean streamwise velocity $\overline{u}(z)$, where U_∞ is the incoming velocity at hub height and U is the depth averaged velocity. Figure 2b provides the streamwise turbulent intensity u_{rms}/u_*, where u_{rms} is the root-mean-square of the streamwise velocity fluctuations normalized by the shear velocity u_*. This latter was estimated with the Energy-gradient method for uniform flows $u_* = \sqrt{gR_H S_w}$, where R_H is the hydraulic radius, g is the gravitational acceleration (9.81 ms^{-2}), and S_w is the water surface slope measured using the Massa sensor. The shear velocity resulting from the energy gradient was observed to vary between 0.018 and 0.025 $\mathrm{m\ s}^{-1}$ in all the experiments performed (leading to a mean value $u_* = 0.022\ \mathrm{m\ s}^{-1}$). This estimate compared reasonably well with $u_* = 0.015\mathrm{m\ s}^{-1}$ obtained with the Clauser method, i.e. by fitting a logarithmic velocity distribution $\frac{u}{u_*} = \frac{1}{k}\ln(\frac{z}{z_0})$ where $k = 0.41$ is the Von Karman constant, and z_0 is the estimated aerodynamic roughness length (Clauser 1956). However given the limited number of data points in the logarithmic layer, we decided to impose $u_* = 0.022\ \mathrm{m\ s}^{-1}$ calculated from the energy method, and use the logarithmic law to estimate the roughness length, leading to $z_0 = 3 \times 10^{-5}$ m. The estimated z_0 ultimately suggests a sand equivalent roughness $k_s \approx 0.9 \times 10^{-3}$ m ($z_0 = 0.033\ k_S$, see Jiménez (2004)) very similar to our median grain size $d_{50} = 1.13 \times 10^{-3}$ m.

Following the procedure proposed by van Rijn (1984) (based on the original work by Shields (1936)), the Shields diagram provides the critical mobility parameter $\theta_{cr} =$ 0.034 associated with our median grain diameter d_{50}. With the above estimated u_*, the Shields parameter for the grain mobility is calculated as $\theta = u_*^2/[(s-1)gd_{50}] = 0.027$, where s is the sand to water density ratio $s = \rho_s/\rho_w = 2.65$. The clear water conditions are therefore confirmed as $\theta < \theta_{cr}$. We also calculated the critical flow velocity according to Melville and Sutherland (1988). Specifically, $U_c = u_{*_c} 5.75\ \log(5.53\frac{h}{d_{50}})$, where h is the flow depth and u_{*_c} the critical shear velocity $u_{*_c} = \sqrt{\frac{\tau_{cr}}{\rho_w}} = 0.025\ \mathrm{m\ s}^{-1}$. The resulting critical flow velocity $U_c = 0.45\mathrm{m\ s}^{-1}$ is higher than our mean flow velocity

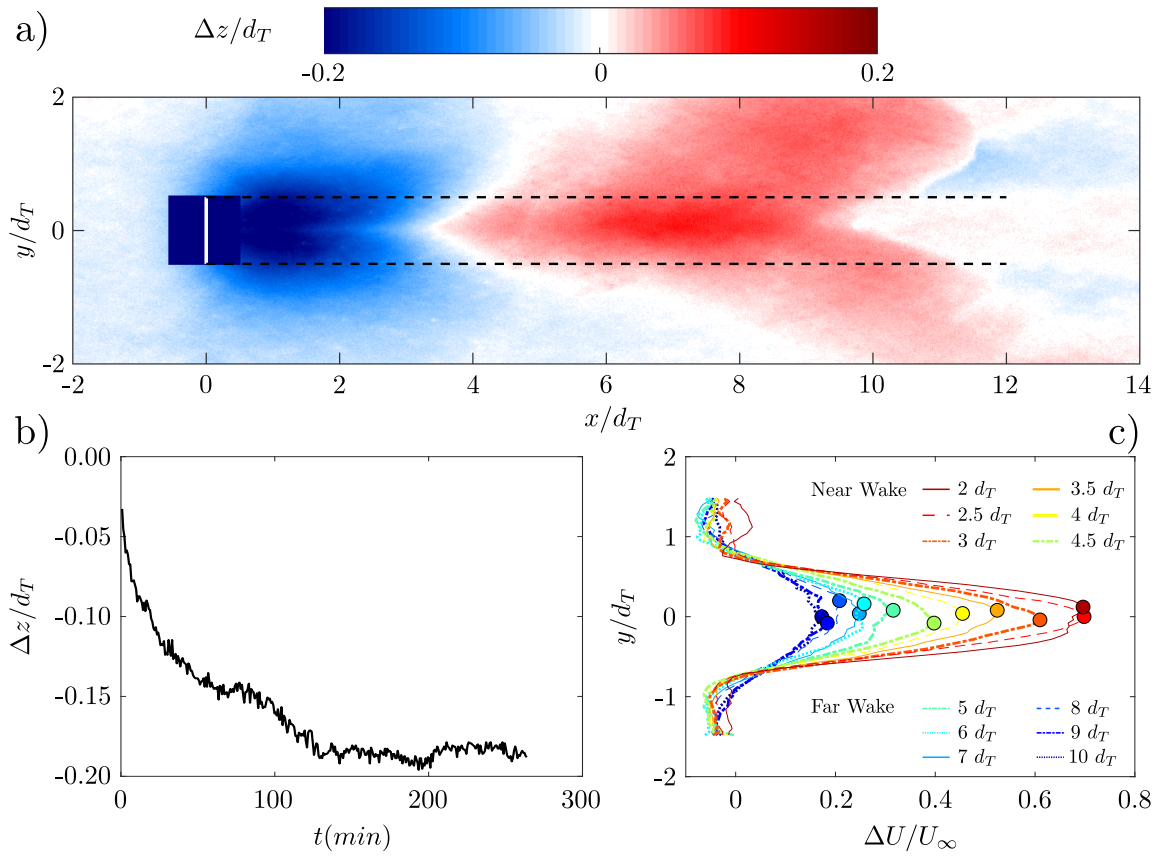

FIG. 3. Experimental procedure: a) bathymetry $z(x, y)$ at equilibrium conditions, b) temporal evolution of the local scour to assess equilibrium conditions, and c) mean velocity profile in the turbine wake. Data refer to the reference case with the turbine centered in the channel cross-section, $\phi_T = 0°$ and clockwise blade rotation. Note that the white line in panel a) and in the following figures refers to the rotor location and orientation, while the rectangle surrounding the rotor plane is a region where the laser was sheltered by the turbine nacelle, preventing the measurements.

$U = 0.40\ \mathrm{m\ s^{-1}}$, thus confirming the clear-water condition. Furthermore, note that the value of the critical shear velocity u_{*_c} obtained following Melville (1997) leads to $u_{*_c} = 0.027\ \mathrm{m\ s^{-1}}$, similar to the above estimate. Note that clear water conditions were also monitored during the experiment by visually inspecting the bed. At the beginning of each experiment the bed was flattened and the ADV was positioned for 10 min in the center of the channel 1 m upstream of the turbine to monitor the averaged velocity at hub height, as a boundary condition. Meanwhile, bed and water surface elevation streamwise profiles were repeatedly measured to monitor the depth and the corresponding slopes.

RESULTS

Centered turbine

The first set of experiments was performed with the turbine placed in the center of the channel, $y = 0$, focusing on the effect of the yaw angle on the local bathymetry and on the spatial evolution of the turbine wake (Figure 4). The reference, centered, turbine experiment is performed at $\phi_T = 0°$, and clockwise blade rotation, as tested by Hill et al. (2014) and shown in Figure 3.

In the reference conditions, the scour region extends approximately 3 d_T in the longitudinal downstream direction and 2 d_T in the spanwise direction, symmetrically with respect to the turbine location (Figure 3a). This local geomorphic signature is qualitatively similar to the bridge pier scour, but augmented due to the additional shear stress induced by the rotor. The phenomenology of the scour mechanism is amply discussed in the predictive modeling work by Musa et al. (2018a). As a results of the critical mobility conditions, sediments eroded from the scour region were transported and deposited downstream in a chevron shaped dune, extending up to 11 d_T - 12 d_T. The maximum scour and deposit were estimated as -0.23 and 0.10 times the rotor diameter d_T respectively. The temporal convergence of the scour-deposition process is

shown in Figure 3b where the bed evolution at $x/d_T = 0.7$ and $y/d_T = 0$ is plotted in time. Both the scour and the deposit, were observed to develop significantly in the first 60 min and reach a stable value around $t \approx 130$ min, which is significantly shorter than the duration of all the experiments. We acknowledge we have not always monitored the scour evolution in time and assessed the equilibrium conditions; first, all the experiments were performed under the same flow conditions, implying that the temporal evolution of scour-deposition processes should be similar; second, as the scour depth decreases with increasing yaw angle (no matter which direction), the equilibrium time $t = 130$ min estimated for the maximum scour configuration is regarded as a conservative estimate.

Using the mean velocity component along the x-axis, $U(x)$, the corresponding deficit value $\Delta U(x) = U_\infty - U(x)$ was calculated, where U_∞ is the, undisturbed, spanwise averaged velocity at hub height upstream of the turbine, also defined as hub velocity. In Figure 3c, the dimensionless deficit profiles $\Delta U/U_\infty$, are plotted as a function of x, y, with the location of the maximum velocity deficit (or minimum velocity) marked as a symbol and consistently located in the proximity of the centerline. Note that this is not significantly affected by the direction of rotation of the rotor (not shown). To provide a visual of the yaw angle effects on both the local scour-deposition features and the wake, the spanwise profiles of $\Delta U/U_\infty$ at 6 d_T downstream of the turbine are plotted in Figure 4 and superimposed on the final bathymetry for all the yaw angles investigated. The wake orientation is steered in the opposite direction of the rotor yaw. Specifically, as the turbine is negatively yawed (panels a,b,c), the wake is observed to steer in the opposite direction with the velocity minima shifting towards the left side of the channel (top side of the plot), and vice versa (panels d,e,f). This finding agrees well with all the existing wake models for yawed wind turbines (Jiménez et al. 2010; Bastankhah and Porté-Agel 2016; Dou et al. 2019a). The wake distortion is attributed to the coexistence of a drag force acting on the flow in the x-direction and

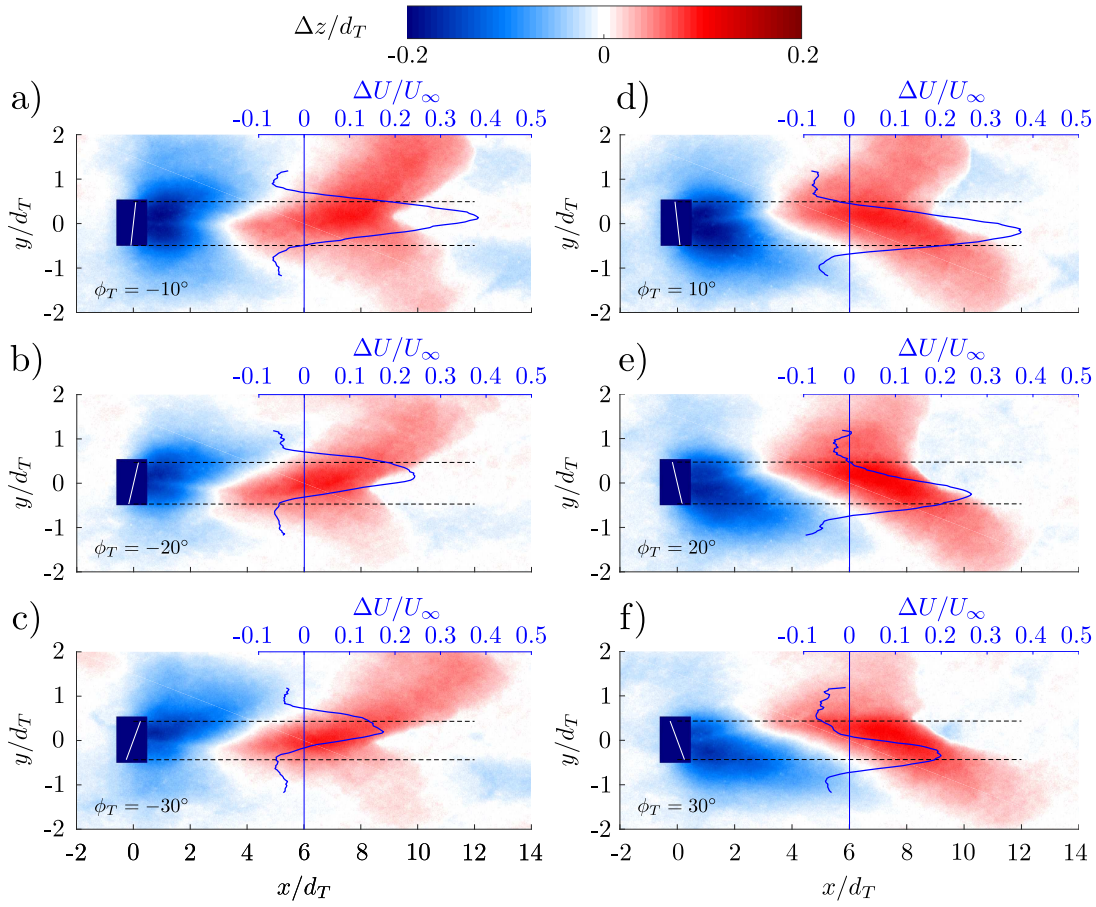

FIG. 4. Span wise profile of the mean velocity deficit (blue line and blue top axis) at 6 d_T downstream of the turbine, superimposed on the final bathymetry, for each yaw angle; from top to down panels $\phi_T = -10°$, $-20°$, $-30°$ (a,b,c) and $10°$, $20°$ $30°$ (d,e,f).

a thrust component applied in the skew direction of the rotor plane, which acts on the flow passing through the rotor and distort the wake. However, it is quite surprising that the scour seems to follow closely the rotor orientation with the crest edge, along which sediments are eroded and transported downstream, perpendicular to the yawed rotor plane. This suggests that the wake flow at hub height, is counteracting the near-wake hydrodynamics close to the bed surface and the support tower (or vice versa). For the

negatively yawed cases for instance, the sediments that are ejected towards the right hand side of the channel (the lower boundary in Figure 4) start forming a deposit, at about $4d_T$, that is initially skewed with respect to the tower, but then tilts progressively towards the wake minima, as the velocity slows down and sediments stop moving.

The spatial evolution of the wake is further highlighted in Figure 5a-b where the velocity minima clearly indicate a significant distortion of the wake. In Figure 5c the spatial evolution of those points is plotted against the theoretical prediction of Dou et al. (2019a), suggesting that axial flow MHK turbines behave in the same way of axial flow wind turbines. According to the simplified model by Dou et al. (2019a), tested on wind turbine models, the general offset model for yaw angles lower then 30° is expressed as, (1):

$$\frac{Y_o}{d_T} = \delta[C_T(\phi_T = 0^\circ)\sin\phi_T]^\zeta \cos^{2\zeta}\phi_T \sqrt{\frac{x}{d_T}} + \frac{d_{rt}}{d_T}\sin\phi_T \tag{1}$$

where Y_o is the spanwise distance, i.e. the offset, between the position of the maximum velocity deficit and the centerline ($y/d_T = 0$), δ and ζ are two coefficients of the model, equal to 0.74 and 0.83 respectively (in the original formulation), C_T is the thrust coefficient for a turbine with yaw angle equal to 0° and d_{rt} is the distance between the rotational center of the tower and the hub center in the y-direction. For our MHK turbine model, $d_{rt} = 36$ mm and C_T, for yaw angle equal to 0° is 0.74 (see drag measurement performed in Musa et al. (2018b)). The parameter ζ was kept equal to 0.83 as suggested by Dou et al. (2019a), while δ was calibrated to 0.35. In Figure 5c the colored lines represent the model predictions, while the symbols mark the estimated locations of the maximum velocity deficit obtained interpolating the experimental data with a Gaussian curve in the close proximity of the peak to improve the estimate of the wake center. The percentage error between the experimental data and the model prediction is based on the spanwise location of the velocity minima at hub height, de-

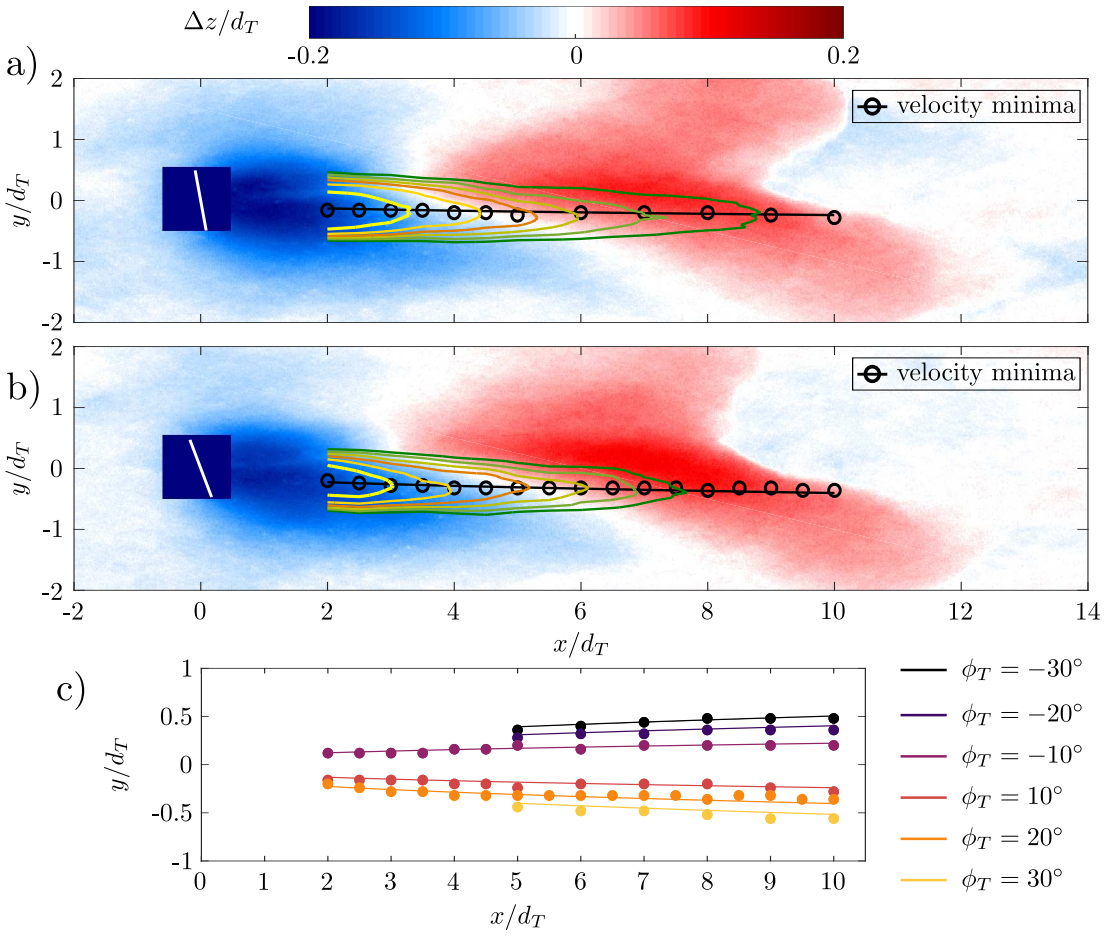

FIG. 5. Mean velocity deficit isolines with minimum velocity marked and plotted over the final bathymetry for yaw angles a) $\phi_T = 10°$ and b) $\phi_T = 20°$, respectively. c) Comparison between the location of the velocity minima at increasing x/d_T (dots) and the model by Dou et al. (2019a) (lines), described in equation 1. The vertical order of the lines in the legend is the same as the lines in the plot.

fined as Y_o, and are calculated as $e_\phi[\%] = \langle|(Y_o^d - Y_o^m)/Y_o^m|\rangle * 100$. Y_o^d is evaluated on the experimental data, Y_o^m is the model prediction, the vertical lines indicate the absolute value and the angle brackets the average. The percentage errors are: $e_{-30°} =$

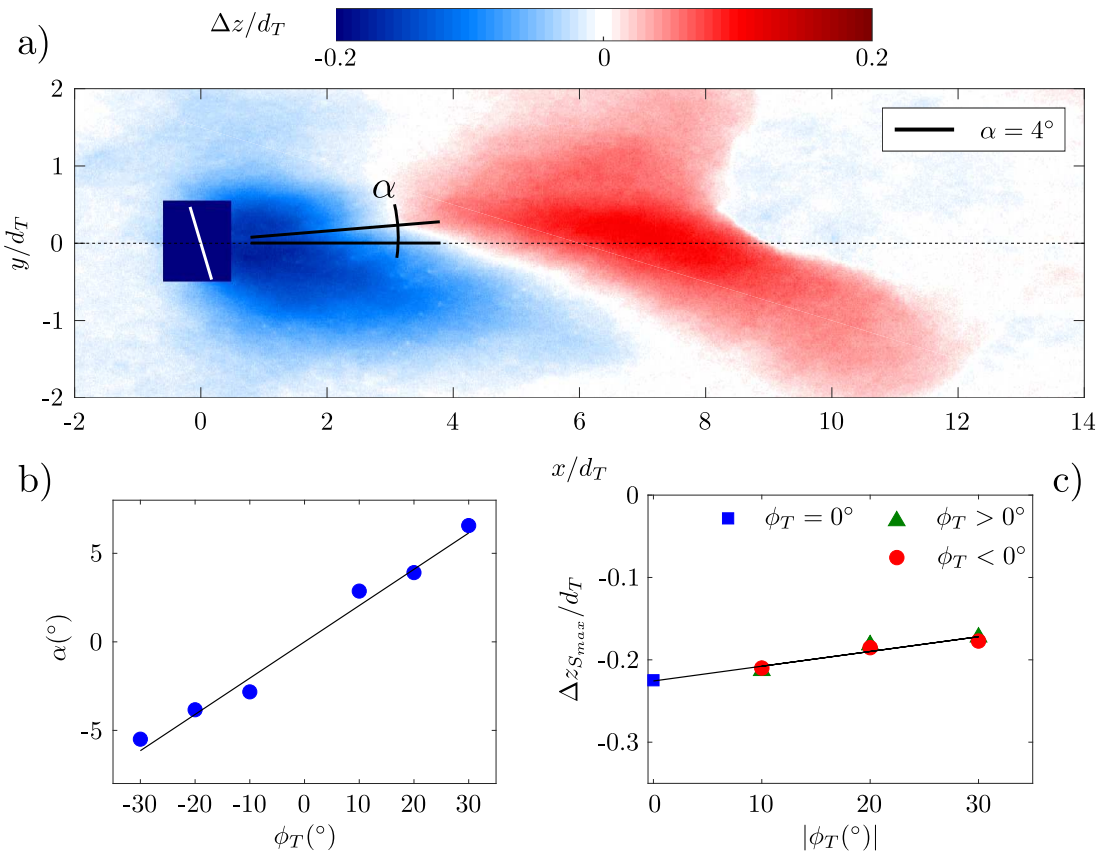

FIG. 6. Summary of the bathymetric effects due to yaw angle orientation: a) final topography for $\phi_T = 20°$, b) scour crest angle α and c) maximum scour depth $\Delta z_{S_{max}}$ for the tested yaw angles. α is defined as the angle between the characteristic scour crest and the turbine y-location (in this case $y = 0$).

277 4%, $e_{-20°} = 7\%$, $e_{-10°} = 9\%$, $e_{10°} = 12\%$, $e_{20°} = 8\%$, $e_{30°} = 10\%$. Please note that
278 the formulation by Dou et al. (2019a) has been recently updated providing a more thor-
279 ough evaluation of the parameters, and the extension to non-Gaussian, skewed, wake
280 profiles for both wind and MHK turbines (Dou et al. 2019b).

281 The effect of the yaw angle ϕ_T on the riverbed configuration is described in Figure

6 by measuring: i) the deviation of the monopile scour crest from the $\phi_T = 0°$ symmetric case, defined by the angle α (Figure 6a,b), and ii) the maximum scour depth $\Delta z_{S_{max}}$(Figure 6a,c). In particular, the scour crest, which delimits the two lobes of the local scour region and coincides with $y/d_T = 0$ for $\phi_T = 0°$, was identified as the local maxima of the detrended bed elevation in the scour region. The angle α was calculated as the angle between linearly interpolated maxima and the center of the channel $y/d_T = 0$ (i.e. the turbine tower y-location, see Figure 6a). Results plotted in Figures 6b,c denote robust statistical trends regardless of the blade rotational direction (confirming the minimal changes in key bathymetric variables summarized in Table 2).

The effect of the yaw angle on the the flow field and the turbine performance was quantified by measuring the wake deficit longitudinal profile ΔU (Figure 7a) and the mean voltage V (Figure 7b), respectively. With increasing yaw angle the turbine performance, as well as the thrust coefficient estimated in a towing tank experiment (not shown here) are reduced, resulting in a weaker velocity deficit. Figure 7a shows a reduction in the velocity deficit as the yaw angle increases, both in the near and the far wake. Note that for $\phi_T = 30°$, points measured at $x/d_T < 5$ do not follow the expected trend and were distinguished by white markers. We infer that as the yaw angle increases, the wake is periodically disrupted: perhaps stalling at specific blade cross section and resulting in lift, circulation and tip vortex drops, followed by influx of high momentum fluid in the wake. This could contribute to increase the unsteadiness of the near wake, affecting the convergence and/or the reliability of our measurements close to the rotor plane.

Consistent with the velocity deficit reduction, Figure 7b shows the mean voltage V, normalized by the corresponding measurement from the zero-yaw turbine V_0. Note that the voltage output is linearly proportional to the rotor angular velocity, as demonstrated in Musa et al. (2018b) and verified here in selected cases using underwater video recording. Therefore, the mean voltage ratio, resulting from continuously mea-

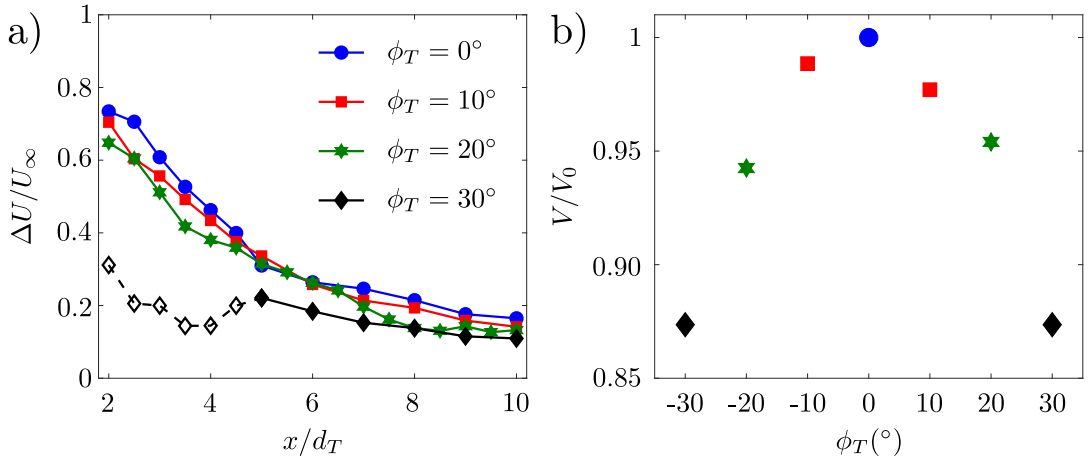

FIG. 7. Summary of the performance changes due to yaw angle orientation: a) velocity deficit ΔU normalized by the incoming flow at hub height U_∞ and b) rotor mean voltage V normalized by the mean voltage from the zero-yaw turbine V_0. White markers in panel a) represent points that do not follow the expected wake trend, potentially due to wake periodical disruptions caused by the yaw angle.

sured voltage time series for the whole duration of the experiments, represents here the ratio of averaged angular velocity and a simplified, though robust, metric for turbine comparative performance.

A smaller thrust coefficient and a reduced wake deficit imply that, with increasing yaw angles, the shear stress augmentation downstream of the foundation tower is reduced, and thus the scour. The crest orientation in the scour region reveals a clear dependence on the yaw angle, exhibiting a direction fairly normal to the rotor and opposite to the orientation of the velocity minima line. The next step is to verify that the above findings hold when the turbine is located closer to a side wall, which might present opportunities for potential passive control strategies to enhance or mitigate

stream bank erosion.

Near-bank turbine

In this second set of experiments the MHK turbine was located in the proximity of the left hand side channel wall as described in the Experimental Apparatus section. The main goal is to investigate the opportunity to steer the wake away from the side wall and favor sediment deposition towards the stream bank. Both processes would contribute to protect the river from lateral erosion. Two yaw angles (-20° and 20°) and two rotational directions cases are investigated, in addition to the un-yawed, near bank, reference case. First, the mean velocity contours in the wake up to 10 d_T is included in Figure 8. While the aligned rotor generates a fairly symmetrical wake, the two yawed configurations reproduced a distorted and skewed wake, consistent with the previous observations. In particular, note that with the $\phi_T = 20^\circ$ configuration, the wake is steered towards the center of the channel, thus likely preventing the rotor annular shear layer to impinge on the side wall (Figure 8c). The same configuration is observed to promote the transport of eroded sediments from the scour occurring near the support tower towards the side wall while keeping the maximum scour away from it (Figure 9c).

In order to make a final assessment on the efficiency of the depositional mechanism, the centroid of the whole deposit Δy_C is estimated with respect to the side wall line and is identified in a subregion $1 < x/d_T < 11$ and $0 < y/d_T < 3$, weighted on the actual bed elevation (above a threshold $\Delta z/d_T > 0.01$). In figure 9 the deposit centroid is found to be located closer to the side bank for the $\phi_T = 20^\circ$, with only second order effects from the blade rotational direction. The final configuration of the deposit skewed shape for different yaw angles qualitatively resembles the centered turbine cases and the maximum scours are slightly reduced in comparison to the reference centered turbine at $\phi_T = 0^\circ$ (see Table 2). However, the implications of partially

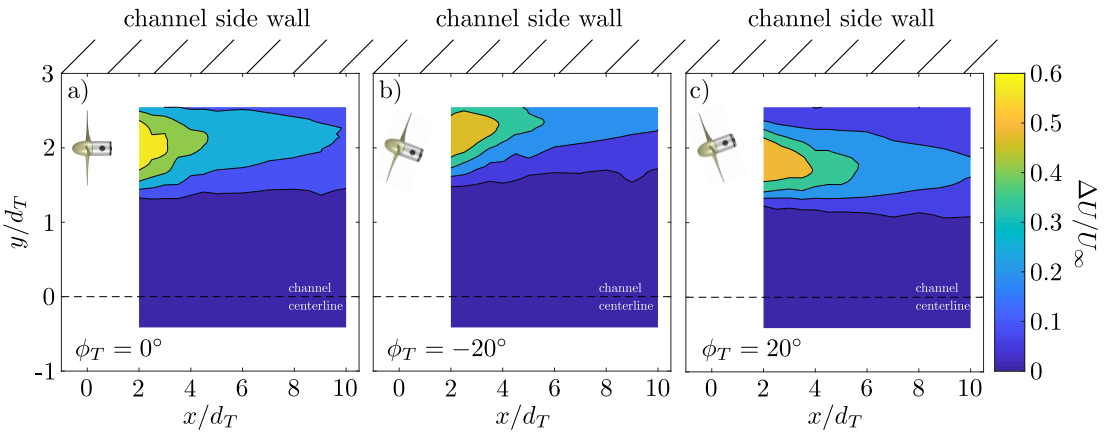

FIG. 8. Mean velocity deficit contour $\Delta U/U_\infty$ in the wake of a turbine installed close to the side wall, for different yaw angles: a) $\phi_T = 0°$, b) $\phi_T = -20°$, c) $\phi_T = 20°$.

steering depositional patterns by prescribed MHK turbine yaw angle misalignment are far more interesting.

DISCUSSION

Musa et al. (2018b) demonstrated that axial flow turbines can be safely deployed in large scale rivers with intense sediment transport and large migrating bedforms. A specific turbine array siting was designed to minimize large-scale non-local morphodynamic effects while keeping navigability on one side of the channel. In the follow-up work, Musa et al. (2019) tested a vane-like turbine array configuration to deflect the core of the flow to promote morphodynamic effects and meandering onset. Those efforts were based exclusively on turbine siting. Here, results show that by yawing a single MHK turbine it is possible to govern the wake, steering it away from the channel side banks and favoring deposition towards the wall. The same strategy can be applied to steer the wake away from downstream turbines and maximize the power plant performance, as suggested in the wind energy community (Boersma et al. 2017),

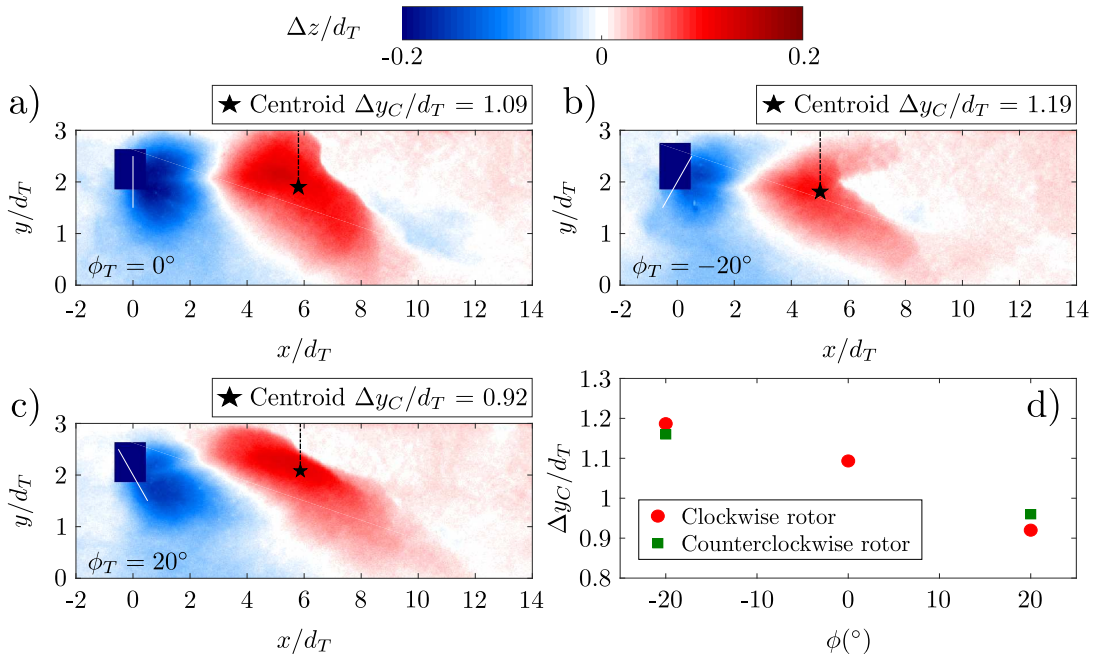

FIG. 9. Final topography scan for the side-wall turbine case at different yaw angles: a) $\phi_T = 0°$, b) $\phi_T = -20°$ and c) $\phi_T = 20°$. d) Normalized deposit centroid distance from the wall Δy_C as function of the yaw angle and blade rotational direction for all the tested cases.

yet the implications on large scale fluvial evolution are far more intriguing. This and the above benchmark experiments are devoted to provide a set of guidelines to expand renewable energy production in rivers with minimal environmental impacts. The current results, in particular, may provide the first example of positive environmental impact, consisting in the protection from bank erosion by opportunely sited and yawed hydrokinetic turbines, while producing renewable energy. While we acknowledge that a MHK turbine near the bank still induces a local scour, we have shown that the non-local, or far-wake, effects are both contributing to mitigate streambank erosion: steering the wake away from the lateral wall, is expected to reduce the mean shear and the Reynolds stresses on the sidewall boundary layer; steering the deposit

towards the back is expected to supply erodible material and limit near bank scour. Further investigation should be devoted to test a streamwise array of yawed turbines near the bank to confirm the current results and assess if the collective behavior of multiple yaweds rotor could provide an effective shelter along a river meander. River management in urbanized environments is a challenging task that needs to take into account human (and human structures) safety along with the improvement of physical and ecological conditions of often degraded urban streams (Bernhardt and Palmer 2011; Wohl et al. 2015). A complete restoration of the natural forms and processes is often not achievable, because of conflicting river ecosystem services. However, efforts can be made to diversify streambank protection strategies. This study suggests that it is possible to positively couple renewable energy production and bank protection, taking advantage of the turbine downstream deposit to integrate and/or substitute more established techniques based on roughness, vegetation patches, vanes, or other more or less invasive hydraulic structures (Henderson 1986; Odgaard and Mosconi 1987; Odgaard and Wang 1991b; Maynord 1995; Froehlich and Benson 1996; Allen and Leech 1997; Li and Eddleman 2002).

CONCLUSION

An axial flow Hydrokinetic Turbine has been tested in yawed conditions to explore potential passive control strategies to produce renewable energy from river flows, while protecting the banks from erosion. Experiments were carried out in critical mobility conditions to explore the parameter space through relatively short experiments. Results with the turbine deployed along the channel centerline show that yaw angle variations induce a deflection of the wake and consequently affect the near-wall, near-wake direction of the scour and sediment transport, the maximum scour depth, and the size and orientation of the deposit. In terms of performance, the angular velocity of the turbine is slightly reduced, while the turbine blade rotational direction (clockwise or

counterclockwise) was shown to have negligible effects on the above quantities and trends. The yawed centered turbine is used here as a reference set of experiments with potential implications on power performance at the MHK array scale, by preventing the wakes to impinge of downstream turbines. When the turbine is located close to the side walls, the qualitative description of the wake and bathymetric evolution is not significantly changed, paving the road to a different set of passive control strategies. In particular, with the turbine rotor positively yawed, the upstream rotor facing the center of the channel, the wake is shown to deflect away from the stream bank while the deposit is observed to move towards the bank. In addition, the local scour is reduced, when compared to the center un-yawed turbine, as a combined effect of lower incoming velocity and yawed rotor. All these mechanisms suggest that opportunely chosen yaw angles could passively reduce streambank erosion with a minimal loss in power production. The limited bedload transport conditions and the absence of migrating bedforms certainly represent the biggest limitations of this work, which however provides the proof of concept needed to move this investigation forward and address the need to better integrate renewable energy devices within the natural environment, as discussed above and in Musa et al. (2019).

DATA AVAILABILITY

Some or all data, models, or code generated or used during the study are available from the corresponding author by request.

ACKNOWLEDGMENTS

This work was supported by National Science Foundation (NSF) Career Grant Geophysical Flow Control (Michele Guala - grant number 1351303) and by Doctoral Dissertation Fellowship awarded to PhD student M. Musa by the University of Minnesota. The authors would like to thank SAFL engineering staff for the constant and professional support.

REFERENCES

Abad, J. D., Rhoads, B. L., Güneralp, İ., and García, M. H. (2008). "Flow structure at different stages in a meander-bend with bendway weirs." *Journal of Hydraulic Engineering*, 134(8), 1052–1063.

Ahmadi, M. H. (2019). "Influence of upstream turbulence on the wake characteristics of a tidal stream turbine." *Renewable energy*, 132, 989–997.

Allen, H. H. and Leech, J. R. (1997). "Bioengineering for streambank erosion control. report 1-guidelines.." *Report no.*, Army Eengineer Waterways Experiment Station Vicksburg MS.

Bachant, P. and Wosnik, M. (2015a). "Characterising the near-wake of a cross-flow turbine." *Journal of Turbulence*, 16(4), 392–410.

Bachant, P. and Wosnik, M. (2015b). "Performance measurements of cylindrical-and spherical-helical cross-flow marine hydrokinetic turbines, with estimates of exergy efficiency." *Renewable Energy*, 74, 318–325.

Bahaj, A., Molland, A., Chaplin, J., and Batten, W. (2007). "Power and thrust measurements of marine current turbines under various hydrodynamic flow conditions in a cavitation tunnel and a towing tank." *Renewable energy*, 32(3), 407–426.

Baldwin, S., Bindewald, G., Brown, A., Chen, C., Cheung, K., Clark, C., and Cresko, J. (2015). "Quadrennial technology review 2015: Technology assessments–marine and hydrokinetic power." *Report no.*, United States. Department of Energy. Office of Energy Efficiency and Renewable Energy.

Bane, J. M., He, R., Muglia, M., Lowcher, C. F., Gong, Y., and Haines, S. M. (2017). "Marine hydrokinetic energy from western boundary currents." *Annual review of marine science*, 9, 105–123.

Bastankhah, M. and Porté-Agel, F. (2016). "Experimental and theoretical study of wind turbine wakes in yawed conditions." *Journal of Fluid Mechanics*, 806, 506–541.

448 Bernhardt, E. S. and Palmer, M. A. (2011). "River restoration: the fuzzy logic of re-
449 pairing reaches to reverse catchment scale degradation." *Ecological applications*,
450 21(6), 1926–1931.
451 Boersma, S., Doekemeijer, B., Gebraad, P. M., Fleming, P. A., Annoni, J., Scholbrock,
452 A. K., Frederik, J., and van Wingerden, J.-W. (2017). "A tutorial on control-oriented
453 modeling and control of wind farms." *2017 American Control Conference (ACC)*,
454 IEEE, 1–18.
455 Chamorro, L. P., Hill, C., Morton, S., Ellis, C., Arndt, R., and Sotiropoulos, F. (2013).
456 "On the interaction between a turbulent open channel flow and an axial-flow tur-
457 bine." *Journal of Fluid Mechanics*, 716, 658–670.
458 Chen, L., Hashim, R., Othman, F., and Motamedi, S. (2017). "Experimental study
459 on scour profile of pile-supported horizontal axis tidal current turbine." *Renewable*
460 *Energy*, 114, 744–754.
461 Churchfield, M. J., Li, Y., and Moriarty, P. J. (2013). "A large-eddy simulation study of
462 wake propagation and power production in an array of tidal-current turbines." *Phil.*
463 *Trans. R. Soc. A*, 371(1985), 20120421.
464 Clauser, F. H. (1956). "The turbulent boundary layer." *Advances in applied mechanics*,
465 Vol. 4, Elsevier, 1–51.
466 Dou, B., Guala, M., Lei, L., and Zeng, P. (2019a). "Experimental investigation of the
467 performance and wake effect of a small-scale wind turbine in a wind tunnel." *Energy*,
468 166, 819–833.
469 Dou, B., Guala, M., Lei, L., and Zeng, P. (2019b). "Wake model for horizontal-axis
470 wind and hydrokinetic turbines in yawed conditions." *Applied Energy*, 242, 1383–
471 1395.
472 Fraser, S., Nikora, V., Williamson, B. J., and Scott, B. E. (2017). "Hydrodynamic
473 impacts of a marine renewable energy installation on the benthic boundary layer in
474 a tidal channel." *Energy Procedia*, 125, 250–259.

475 Froehlich, D. C. and Benson, C. A. (1996). "Sizing dumped rock riprap." *Journal of*
476 *Hydraulic Engineering*, 122(7), 389–396.
477 Frost, C., Morris, C. E., Mason-Jones, A., O'Doherty, D. M., and O'Doherty, T. (2015).
478 "The effect of tidal flow directionality on tidal turbine performance characteristics."
479 *Renewable Energy*, 78, 609–620.
480 Galloway, P. W., Myers, L. E., and Bahaj, A. S. (2014). "Quantifying wave and yaw
481 effects on a scale tidal stream turbine." *Renewable energy*, 63, 297–307.
482 Gebraad, P., Thomas, J. J., Ning, A., Fleming, P., and Dykes, K. (2017). "Maximization
483 of the annual energy production of wind power plants by optimization of layout and
484 yaw-based wake control." *Wind Energy*, 20(1), 97–107.
485 Grant, I., Parkin, P., and Wang, X. (1997). "Optical vortex tracking studies of a hori-
486 zontal axis wind turbine in yaw using laser-sheet, flow visualisation." *Experiments*
487 *in fluids*, 23(6), 513–519.
488 Haas, K. A., Fritz, H. M., French, S. P., Smith, B. T., and Neary, V. S. (2011). "Assess-
489 ment of energy production potential from tidal streams in the united states." *Report*
490 *no.*, Georgia Tech Research Corporation, Atlanta, GA (United States).
491 Henderson, J. E. (1986). "Environmental designs for streambank protection projects."
492 *Journal of the American Water Resources Association*, 22(4), 549–558.
493 Hill, C., Kozarek, J., Sotiropoulos, F., and Guala, M. (2016a). "Hydrodynamics and
494 sediment transport in a meandering channel with a model axial-flow hydrokinetic
495 turbine." *Water Resources Research*, 52(2), 860–879.
496 Hill, C., Musa, M., Chamorro, L. P., Ellis, C., and Guala, M. (2014). "Local scour
497 around a model hydrokinetic turbine in an erodible channel." *Journal of Hydraulic*
498 *Engineering*, 140(8), 04014037.
499 Hill, C., Musa, M., and Guala, M. (2016b). "Interaction between instream axial flow
500 hydrokinetic turbines and uni-directional flow bedforms." *Renewable Energy*, 86,
501 409–421.

Howard, K., Hu, J., Chamorro, L. P., and Guala, M. (2015). "Characterizing the response of a wind turbine model under complex inflow conditions." *Wind Energy*, 18(4), 729–743.

Jacobson, P. T., Hagerman, G., and Scott, G. (2011). "Mapping and assessment of the united states ocean wave energy resource." *Report no.*, Electric Power Research Institute.

Jiménez, Á., Crespo, A., and Migoya, E. (2010). "Application of a les technique to characterize the wake deflection of a wind turbine in yaw." *Wind energy*, 13(6), 559–572.

Jiménez, J. (2004). "Turbulent flows over rough walls." *Annu. Rev. Fluid Mech.*, 36, 173–196.

Kang, S., Borazjani, I., Colby, J. A., and Sotiropoulos, F. (2012). "Numerical simulation of 3d flow past a real-life marine hydrokinetic turbine." *Advances in water resources*, 39, 33–43.

Kang, S., Yang, X., and Sotiropoulos, F. (2014). "On the onset of wake meandering for an axial flow turbine in a turbulent open channel flow." *Journal of Fluid Mechanics*, 744, 376–403.

Khosronejad, A., Hill, C., Kang, S., and Sotiropoulos, F. (2013). "Computational and experimental investigation of scour past laboratory models of stream restoration rock structures." *Advances in water resources*, 54, 191–207.

Lam, W.-H., Chen, L., and Hashim, R. (2015). "Analytical wake model of tidal current turbine." *Energy*, 79, 512–521.

Li, M.-H. and Eddleman, K. E. (2002). "Biotechnical engineering as an alternative to traditional engineering methods: A biotechnical streambank stabilization design approach." *Landscape and Urban Planning*, 60(4), 225–242.

Lust, E. E., Flack, K. A., and Luznik, L. (2018). "Survey of the near wake of an axial-flow hydrokinetic turbine in quiescent conditions." *Renewable Energy*, 129, 92–101.

529 Maganga, F., Germain, G., King, J., Pinon, G., and Rivoalen, E. (2010). "Experimental
530 characterisation of flow effects on marine current turbine behaviour and on its wake
531 properties." *IET Renewable Power Generation*, 4(6), 498–509.
532 Maynord, S. T. (1995). "Gabion-mattress channel-protection design." *Journal of hy-*
533 *draulic engineering*, 121(7), 519–522.
534 Medici, D. and Alfredsson, P. (2006). "Measurements on a wind turbine wake: 3d
535 effects and bluff body vortex shedding." *Wind Energy: An International Journal for*
536 *Progress and Applications in Wind Power Conversion Technology*, 9(3), 219–236.
537 Melville, B. and Sutherland, A. (1988). "Design method for local scour at bridge piers."
538 *Journal of Hydraulic Engineering*, 114(10), 1210–1226.
539 Melville, B. W. (1997). "Pier and abutment scour: integrated approach." *Journal of*
540 *Hydraulic Engineering*, 123(2), 125–136.
541 Modali, P. K., Kolekar, N. S., and Banerjee, A. (2018). "Performance and Wake Char-
542 acteristics of a Tidal Turbine under Yaw." *International Marine Energy Journal*,
543 1(1), 41–50.
544 Morandi, B., Di Felice, F., Costanzo, M., Romano, G., Dhomé, D., and Allo, J. (2016).
545 "Experimental investigation of the near wake of a horizontal axis tidal current tur-
546 bine." *International Journal of Marine Energy*, 14, 229–247.
547 Muljadi, E. and Yu, Y.-H. (2015). "Review of marine hydrokinetic power generation
548 and power plant." *Electric Power Components and Systems*, 43(12), 1422–1433.
549 Musa, M., Heisel, M., and Guala, M. (2018a). "Predictive model for local scour down-
550 stream of hydrokinetic turbines in erodible channels." *Physical Review Fluids*, 3,
551 024606.
552 Musa, M., Hill, C., and Guala, M. (2019). "Interaction between hydrokinetic turbine
553 wakes and sediment dynamics: array performance and geomorphic effects under
554 different siting strategies and sediment transport conditions." *Renewable Energy*,
555 138, 738–753.

Musa, M., Hill, C., Sotiropoulos, F., and Guala, M. (2018b). "Performance and resilience of hydrokinetic turbine arrays under large migrating fluvial bedforms." *Nature Energy*, 3(10), 839.

Myers, L. and Bahaj, A. (2006). "Power output performance characteristics of a horizontal axis marine current turbine." *Renewable energy*, 31(2), 197–208.

Myers, L. and Bahaj, A. (2007). "Wake studies of a 1/30th scale horizontal axis marine current turbine." *Ocean Engineering*, 34(5-6), 758–762.

Nash, S. and Phoenix, A. (2017). "A review of the current understanding of the hydro-environmental impacts of energy removal by tidal turbines." *Renewable and Sustainable Energy Reviews*, 80, 648–662.

National Renewable Energy Laboratory (NREL). "Mhk atlas, <https://maps.nrel.gov/mhk-atlas/>. [Accessed on 22 January 2017].

Neary, V. S., Gunawan, B., and Sale, D. (2013). "Turbulent inflow characteristics for hydrokinetic energy conversion in rivers." *Renewable and Sustainable Energy Reviews*, 26, 437–445.

Neill, S. P., Litt, E. J., Couch, S. J., and Davies, A. G. (2009). "The impact of tidal stream turbines on large-scale sediment dynamics." *Renewable Energy*, 34(12), 2803–2812.

Odgaard, A. J. and Mosconi, C. E. (1987). "Streambank protection by submerged vanes." *Journal of Hydraulic Engineering*, 113(4), 520–536.

Odgaard, A. J. and Wang, Y. (1991a). "Sediment management with submerged vanes. i: Theory." *Journal of Hydraulic Engineering*, 117(3), 267–267.

Odgaard, A. J. and Wang, Y. (1991b). "Sediment management with submerged vanes. ii: Applications." *Journal of Hydraulic Engineering*, 117(3), 284–302.

Parker, G., <http://hydrolab.illinois.edu/people/parkerg/default.asp>. e-book *1D Morphodynamics of Rivers and Turbidity Currents*. Accessed on 19 August 2017.

Piano, M., Neill, S., Lewis, M., Robins, P., Hashemi, M., Davies, A., Ward, S.,

583 and Roberts, M. (2017). “Tidal stream resource assessment uncertainty due to flow
584 asymmetry and turbine yaw misalignment.” *Renewable Energy*, 114, 1363–1375.
585 Ramírez-Mendoza, R., Amoudry, L., Thorne, P., Cooke, R., McLelland, S., Jordan, L.,
586 Simmons, S., Parsons, D., and Murdoch, L. (2018). “Laboratory study on the effects
587 of hydro kinetic turbines on hydrodynamics and sediment dynamics.” *Renewable*
588 *energy*, 129, 271–284.
589 Shields, A. (1936). “Anwendung der aehnlichkeitsmechanik und der turbulenz-
590 forschung auf die geschiebebewegung.” *Report no.*, Preussischen Versuchsanstalt
591 für Wasserbau.
592 Shields Jr, F. D., Copeland, R. R., Klingeman, P. C., Doyle, M. W., and Simon, A.
593 (2003). “Design for stream restoration.” *Journal of Hydraulic Engineering*, 129(8),
594 575–584.
595 Stallard, T., Collings, R., Feng, T., and Whelan, J. (2013). “Interactions between tidal
596 turbine wakes: experimental study of a group of three-bladed rotors.” *Phil. Trans. R.*
597 *Soc. A*, 371(1985), 20120159.
598 Strom, B., Brunton, S. L., and Polagye, B. (2017). “Intracycle angular velocity control
599 of cross-flow turbines.” *Nature Energy*, 2(8), 17103.
600 van Rijn, L. C. (1984). “Sediment transport, part i: Bed load transport.” *Journal of*
601 *Hydraulic Engineering*, 110(10), 1431–1456.
602 Wohl, E., Lane, S. N., and Wilcox, A. C. (2015). “The science and practice of river
603 restoration.” *Water Resources Research*, 51(8), 5974–5997.
604 Yang, X., Khosronejad, A., and Sotiropoulos, F. (2017). “Large-eddy simulation of a
605 hydrokinetic turbine mounted on an erodible bed.” *Renewable Energy*, 113, 1419–
606 1433.
607 Yang, Z. and Copping, A. (2017). *Marine Renewable Energy: Resource Characteriza-*
608 *tion and Physical Effects*. Springer.

Variable	Name	Value	Units
S	Bed slope	0.04	%
h	Water depth	0.27	m
b	Channel width	0.90	m
U	Depth average velocity	0.40	$\mathrm{m\ s^{-1}}$
Q	Flow discharge	0.10	$\mathrm{m^3\ s^{-1}}$
S_w	Water slope	0.03	%
Fr	Froude number	0.26	
Re	Reynolds number	1.22×10^5	
u_*	Shear velocity	0.02	$\mathrm{m\ s^{-1}}$
d_{50}	Median grain size	1.13	mm
U_∞	Incoming velocity at hub height	0.42	$\mathrm{m\ s^{-1}}$
d_T	Turbine rotor diameter	0.15	m
h_{hub}	Turbine hub height	0.13	m

TABLE 1. Turbine, flow, channel and sediment parameters used during the experiments. Note that U is the depth average velocity calculated with the incoming velocity vertical profile, $Q = U(bh)$, $Fr = U/(gh)^{1/2}$ and $Re = Uh/\nu$, where $\nu = 10^-6\ \mathrm{m^2\ s^{-1}}$ is the kinematic viscosity of water.

Yaw angle ϕ_T	Location	Blade rotation	$\Delta z_{Smax}/d_T$	$\Delta z_{Dmax}/d_T$	$\Delta y_C/d_T$
$0°$	Center	Clockwise	-0.230	0.100	-
$0°$	Center	Counterclockwise	-0.188	0.093	-
$10°$	Center	Clockwise	-0.231	0.097	-
$-10°$	Center	Clockwise	-0.210	0.100	-
$20°$	Center	Clockwise	-0.182	0.120	-
$-20°$	Center	Clockwise	-0.185	0.101	-
$30°$	Center	Clockwise	-0.173	0.102	-
$-30°$	Center	Clockwise	-0.177	0.101	-
$0°$	Near Wall	Clockwise	-0.200	0.140	1.91
$20°$	Near Wall	Clockwise	-0.160	0.130	2.08
$20°$	Near Wall	Counterclockwise	-0.150	0.110	2.04
$-20°$	Near Wall	Clockwise	-0.150	0.100	1.81
$-20°$	Near Wall	Counterclockwise	-0.140	0.110	1.84

TABLE 2. Summary of experiments characteristics and main bathymetric effect for the performed experiments, specifically: maximum scour $\Delta z_{Dmax}/d_T$, maximum deposit $\Delta z_{Smax}/d_T$ and deposit centroid distance from lateral wall $\Delta y_C/d_T$ (for Near Wall cases only).